A Wideband 1×3 Filtering Beamforming Network Featuring Input-Reflectionless and Extended Phase Reconfigurability

Yan ZHANG, Hongmei LIU, Yao MENG, Zhongbao WANG

School of Information Science and Technology, Dalian Maritime University, Dalian, Liaoning 116026, China

zhangyan50050@dlmu.edu.cn, lhm323@dlmu.edu.cn

Submitted December 2, 2025 / Accepted June 24, 2026 / Online first July 16, 2026

Abstract. *In the paper, a wideband 1×3 filtering beamforming network (BFN) with extended phase reconfigurability and input-reflectionless feature is presented for the first time by employing three-way reflectionless power divider, switched 0°/180° phase shifter (PS), and multiway polyphase filtering differential phase shifter (D-PS). The three-way power divider and D-PS provide wideband filtering with high frequency selectivity while ensuring an input-reflectionless characteristic across the entire frequency range. Six distinct output phase differences (PDs) can be realized using only three groups of D-PSs in combination with the switched 0°/180° PSs, enabling extended beam directions without additional phase-shifting components added. The designs of the three-way power divider and D-PS are presented, with the D-PS accompanied by derivation of equations and parametric analysis for clarification. To verify, a prototype is fabricated and measured. Measurements verify six differential PDs of –120°, –90°, –30°, 60°, 90°, and 150°. For all six states, the prototype achieves a 3-dB passband bandwidth exceeding 70% with* $|S_{11}|$ *below –10 dB across the entire frequency range. In addition, the fractional bandwidth corresponding to a ±7° PD error reaches 40%.*

Keywords

Beamforming network, filtering, input reflectionless, phase reconfigurability, multiway polyphase phase shifter

1. Introduction

Multibeam antennas, capable of high-precision beamforming and effectively improving spectrum utilization and coverage, are extensively utilized in wireless communication and radar systems [1], [2]. The beamforming network (BFN) is a critical component of the multibeam antenna front-end, providing excitations with specific amplitude and phase distributions, thereby generating radiation beams in different spatial directions [3–7].

In a multibeam antenna system, the output phase difference (PD) of the BFN directly determines the beam directions of the antenna array. A greater number of beam directions leads to wider coverage and higher positioning accuracy. For conventional BFNs, such as the Butler matrix and Nolen matrix, the number of output PD states is limited by the number of input ports. However, increasing the number of output PD states significantly raises the circuit complexity and insertion loss (IL). Consequently, PD-tunable BFNs have become a research hotspot in recent years, as they can provide more beam directions without introducing additional components. Common design approaches include adding tunable phase shifters (PSs) to the output ports of BFNs [8], or replacing the phase-delay lines inside the BFNs with tunable PSs [9–11]. Although a full 360° continuous phase shift can be obtained [8–11], they feature the drawbacks of narrow fractional bandwidth (FBW) of less than 25% [9–11], and large PD deviation (> ±13°) [8–11], restricting their application for wideband systems.

To overcome these problems, reconfigurable BFNs are proposed [12–14]. In [12], a reconfigurable BFN with eight PDs is constructed by combining asymmetrical 4×4 Butler matrix with single-pole double-throw switches. Although miniaturization can be achieved, the inconsistent number of switches in some paths leads to unequal output power distribution. Moreover, the issues of large IL and phase delay introduced by switches still need to be improved. Subsequently, the reconfigurable coupler is used to form the Butler matrix [13], and the number of beams increases significantly from $2N$ to $3 \times 2N$, with good in-band isolation. However, the PD error is still large (±12°) and deteriorates rapidly with frequency shift, indicating that it is not suitable for wideband systems. Then, an extended Nolen matrix is achieved by a standard 3×3 Nolen matrix cooperating with the single-pole multi-throw switch-based PSs [14]. Six different PDs can be obtained with PD error of lower than ±8.5°, but the cascaded structure increases the overall size.

In addition to the reconfigurable feature, BFNs with integrated filtering characteristics have received increasing

DOI: 10.13164/re.2026.0349

attention, as they can provide signal selection and harmonic suppression. In [15] and [16], coupled resonators were employed to construct filtering BFNs. Although a filtering response with low IL was achieved, these designs suffer from a narrow operating FBW of less than 15% and complex multi-layer structures. The work in [17] utilized a wideband coupler with inherent filtering characteristics to construct a 3×3 BFN, achieving a 3-dB passband bandwidth of over 50% on a single layer. However, it suffers from fixed output PDs. Beyond providing filtering responses, reflectionless circuits offer a key advantage, that is to absorb out-of-band signals instead of reflecting them [18], [19]. This feature effectively improves overall system stability.

This paper presents, for the first time, a wideband 1×3 filtering BFN featuring extended phase reconfigurability and an input-reflectionless characteristic, which is realized by a three-way reflectionless power divider, three switched 0°/180° PSs, and a multiway polyphase filtering differential phase shifter (D-PS). The three-way reflectionless power divider can offer three in-phase output signals with equal amplitude distributions, providing the 3-dB passband FBW of 102%. The multiway polyphase filtering D-PS exhibits differential phase shift range of 0° ~ 180° under the 3-dB passband FBW of 76% and RC of 1.38. The switched 0°/180° PSs enable a total of six output PDs using only three groups of D-PSs, where significantly improving the design flexibility and circuit utilization. The measured results verify six differential PDs of –120°, –90°, –30°, 60°, 90°, and 150°, with the prototype achieving a 3-dB passband FBW exceeding 70%, $|S_{11}|$ below –10 dB across the whole band, and an FBW corresponding to a ±7° PD error of 40%.

2. Design and Implementation of the Proposed BFN

Figure 1 illustrates the topology of the proposed 1×3 filtering BFN. It comprises of a three-way reflectionless power divider, three switched 0°/180° PSs, and a multiway polyphase filtering D-PS with cascaded switches on both sides. Specifically, the three-way reflectionless power divider provides three output signals with equal power and phase, while ensuring an input-reflectionless characteristic. The switched 0°/180° PS enables 0° or 180° output phase by controlling a pair of cascaded switches. Furthermore, the multiway polyphase D-PS comprises one reference line and five main lines (PS_1 − PS_5 in Fig. 1), which are divided into three groups: the reference line, $PS_{1–3}$, and $PS_{4–5}$. Each group shares input and output ports, and the operating mode of the PSs is selected by controlling the on/off states of the paired switches cascaded on both sides.

Table 1 presents all output PD states generated by the proposed BFN under different switch combinations when the relative phase shift values between the main lines PS_1 –PS_5 and reference line are 30°, 90°, 120°, 60°, and 180°,

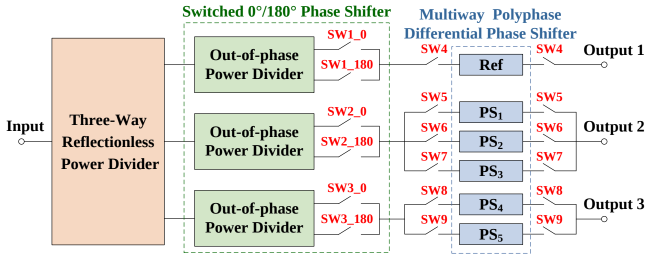

Fig. 1. Topology of the proposed 1×3 BFN.

	State 1 (–30°)	State 2 (150°)	State 3 (–90°)	State 4 (90°)	State 5 (–120°)	State 6 (60°)
SW1_0	On	Off	On	Off	Off	On
SW1_180	Off	On	Off	On	On	Off
SW2_0	On	On	On	On	Off	Off
SW2_180	Off	Off	Off	Off	On	On
SW3_0	On	Off	On	Off	On	Off
SW3_180	Off	On	Off	On	Off	On
SW4	On					
SW5	On		Off		Off	
SW6	Off		On		Off	
SW7	Off		Off		On	
SW8	On		Off		On	
SW9	Off		On		Off	

Tab. 1. Relationship between output phase differences and P-i-n switches.

respectively. It can be observed that, by employing the switched 0°/180° PSs, a total of six output PDs (−120°, −90°, −30°, 60°, 90°, and 150°) can be achieved using only three groups of PSs. Subsequently, according to (1), when the spacing between adjacent elements in antenna array is 0.5λ, the radiation direction θ_M of the antenna array are −41.81°, −30°, −9.59°, 19.47°, 30°, and 56.44°, separately. Here, α and d denote the PD and spacing between adjacent elements in the antenna array, respectively, λ is the wavelength in free space. If other radiation directions are needed, the main lines with other phase shift values can be selected. Furthermore, the number of output ports can be extended by cascading power divider and employing unequal power distribution design method.

$$\theta_M = \arcsin\left(\frac{\alpha\lambda}{2\pi d}\right) \qquad (1)$$

The designs of the three-way reflectionless FPD and the multiway polyphase filtering D-PS are presented in the following, which contribute to the wideband filtering and input-reflectionless characteristics of the BFN. The switched 0°/180° PS is implemented using a slotline transition structure [20], [21].

2.1 Design of the Compact Three-way Reflectionless Power Divider

Figure 2 gives the schematic of the three-way reflectionless power divider, which consists of a five-coupled-line section, three isolation resistors (R_1 and R_2), and a pair of absorptive branches. Each branch comprises an absorptive resistor R_3 and a short-circuited stub with characteristic impedance Z_s. In addition, the electrical lengths of the five-coupled-line (θ) and the short-circuited stubs (θ_{s1}) are both 90°. The five-coupled-line, which is symmetric about the horizontal centerline, can be analyzed as an asymmetrical three-coupled-line (TCL) structure using the even-odd mode decomposition method [18]. After analyzing, the circuit parameters of the designed power divider are as follows: $Z_{oa} = 38\ \Omega$, $Z_{ob} = 33\ \Omega$, $Z_{oc} = 60\ \Omega$, $\Delta Z = 100\ \Omega$ ($\Delta Z = Z_{ea} - Z_{oa} = Z_{eb} - Z_{ob} = Z_{ec} - Z_{oc}$), $Z_s = 80\ \Omega$, $R_1 = 130\ \Omega$, $R_2 = 200\ \Omega$, $R_3 = 63\ \Omega$.

Figure 3 exhibits the *S*-parameters of the three-way reflectionless power divider. As seen in Fig. 3(a), the $|S_{11}|$ remains below −10 dB across the entire band, which is corresponding to the absorption rate ($\gamma = 1 - 10^{|S_{11}|/10}$) of the reflected signal is up to 90%, demonstrating the input reflectionless characteristic is achieved. Furthermore, the

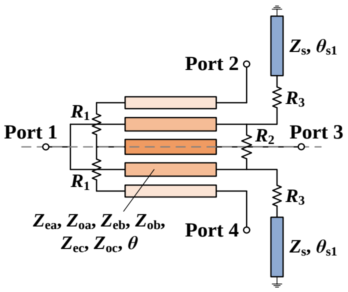

Fig. 2. Schematic of the compact three-way reflectionless FPD.

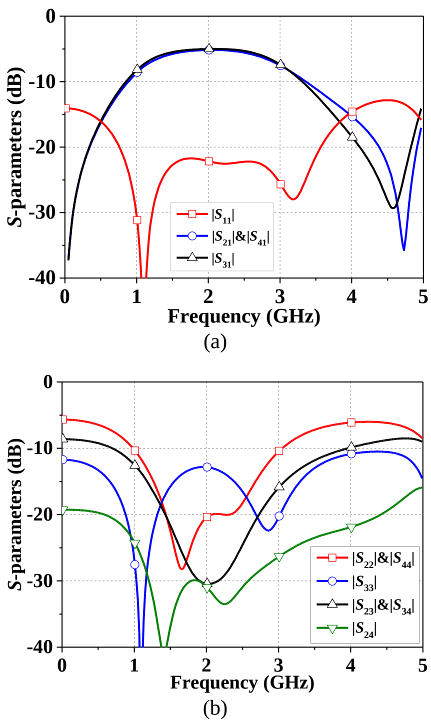

Fig. 3. Simulated results of the proposed three-way reflectionless power divider. (a) Input reflection coefficient and transmission coefficient. (b) Output reflection coefficient and transmission coefficient.

transmission coefficients $|S_{21}|$, $|S_{31}|$, and $|S_{41}|$ each exhibit two transmission zeros (TZs), with a 3-dB FBW of 104% (1.01 GHz ~ 3.09 GHz). As displayed in Fig. 3(b), it also exhibits the good isolation and output impedance matching within the range of 1 GHz to 3 GHz.

2.2 Design of the Multiway Polyphase Filtering D-PS

The schematic of the proposed filtering D-PS is shown in Fig. 4. The reference line comprises of two identical asymmetrical TCL sections and a coupled-line (CL) connected between them, forming a multiple-mode resonator with filtering response. The two types of CLs have even-/odd-mode impedances of Z_{ei} & Z_{oi} (i = 1, 2, 3) and Z_{ec1} & Z_{oc1}, respectively. The electrical lengths of all CLs (θ_1 and θ_2) are 90°, as illustrated in Fig. 4(a). Based on the reference line, two identical delay lines are cascaded on both sides to construct the main line, which has an electrical length of θ_a and characteristic impedance of Z_a. Consequently, the relative PD between the main line and reference line is $-2\theta_a$. Thus, the phase shift range of the proposed D-PS can cover [0, 180°] when the electrical length of delay line θ_a varies from 0° to 90°.

Next, the proposed filtering D-PS is analyzed using the current-voltage method. As illustrated in Fig. 4, the structure can be regarded as a cascade combination of multiple two-port networks. Equation (2) presents the **ABCD**-matrices of these networks, where Z_{mn} (m, n = 1, 2, …, 6) denotes the elements of the **Z** matrix for the asymmetrical TCL [18], and z_{ij} (i, j = 1, 2, 3, 4) represents the elements of the **Z** matrix for the CL [22].

$$[\mathbf{M}_a] = \frac{1}{Z'_{21}} \begin{bmatrix} Z'_{11} & Z'_{11}Z'_{22} - Z'_{12}Z'_{21} \\ 1 & Z'_{22} \end{bmatrix}, \quad (a = 1, 5), \quad (2a)$$

$$[\mathbf{M}_b] = \frac{1}{Z'_{12}} \begin{bmatrix} Z'_{22} & Z'_{11}Z'_{22} - Z'_{12}Z'_{21} \\ 1 & Z'_{11} \end{bmatrix}, \quad (b = 3, 7), \quad (2b)$$

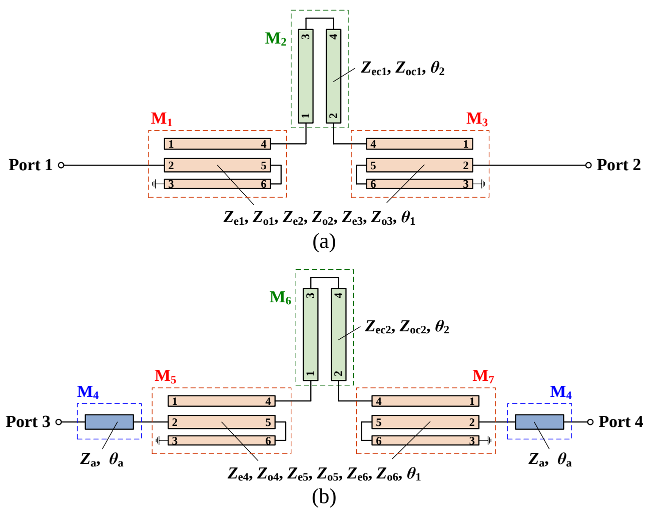

Fig. 4. Schematic of the proposed multiway polyphase filtering D-PS. (a) Reference line. (b) Main line.

$$[\mathbf{M}_c]=\frac{1}{z'_{21}}\begin{bmatrix} z'_{11} & z'_{11}z'_{22}-z'_{12}z'_{21} \\ 1 & z'_{22}\end{bmatrix},\quad (c=2,\,6), \tag{2c}$$

$$[\mathbf{M}_4]=\begin{bmatrix} \cos\theta_a & \mathrm{j}Z_a\sin\theta_a \\ \mathrm{j}\sin\theta_a/Z_a & \cos\theta_a\end{bmatrix} \tag{2d}$$

where

$$Z'_{11}=X_{22}-\frac{(X_{25}-X_{26})(X_{52}-X_{62})}{X_{55}-X_{56}-X_{65}+X_{66}}, \tag{3a}$$

$$Z'_{12}=X_{24}-\frac{(X_{25}-X_{26})(X_{54}-X_{64})}{X_{55}-X_{56}-X_{65}+X_{66}}, \tag{3b}$$

$$Z'_{21}=X_{42}-\frac{(X_{45}-X_{46})(X_{52}-X_{62})}{X_{55}-X_{56}-X_{65}+X_{66}}, \tag{3c}$$

$$Z'_{22}=X_{44}-\frac{(X_{45}-X_{46})(X_{54}-X_{64})}{X_{55}-X_{56}-X_{65}+X_{66}}, \tag{3d}$$

$$X_{mn}=Z_{mn}-\frac{Z_{m3}\cdot Z_{3n}}{Z_{33}},\quad (m,n=1,2,\cdots,6), \tag{3e}$$

$$z'_{11}=z_{11}-\frac{(z_{31}-z_{41})(z_{13}-z_{14})}{z_{33}-z_{34}-z_{43}+z_{44}},\quad z'_{12}=z_{12}-\frac{(z_{32}-z_{42})(z_{13}-z_{14})}{z_{33}-z_{34}-z_{43}+z_{44}},$$
$$z'_{21}=z_{21}-\frac{(z_{31}-z_{41})(z_{23}-z_{24})}{z_{33}-z_{34}-z_{43}+z_{44}},\quad z'_{22}=z_{22}-\frac{(z_{32}-z_{42})(z_{23}-z_{24})}{z_{33}-z_{34}-z_{43}+z_{44}}. \tag{4}$$

Based on (2)–(4), the S-parameters of the reference line and main line can be derived and are expressed in (5).

$$S_{11}=\frac{A_1+B_1/Z_0-C_1Z_0-D_1}{A_1+B_1/Z_0+C_1Z_0+D_1},\ S_{21}=\frac{2}{A_1+B_1/Z_0+C_1Z_0+D_1}, \tag{5a}$$

$$S_{33}=\frac{A_2+B_2/Z_0-C_2Z_0-D_2}{A_2+B_2/Z_0+C_2Z_0+D_2},\ S_{43}=\frac{2}{A_2+B_2/Z_0+C_2Z_0+D_2}, \tag{5b}$$

$$\Delta\Phi=\angle S_{43}-\angle S_{21} \tag{5c}$$

where

$$\mathbf{M}_{\mathrm{Ref}}=\mathbf{M_1M_2M_3}=\begin{bmatrix} A_1 & B_1 \\ C_1 & D_1\end{bmatrix}, \tag{6a}$$

$$\mathbf{M}_{\mathrm{Main}}=\mathbf{M_4M_5M_6M_7M_4}=\begin{bmatrix} A_2 & B_2 \\ C_2 & D_2\end{bmatrix}, \tag{6b}$$

$$O_b=\frac{1}{N}\left\{\sum_{i=1}^{N}\left|S_{11}(f_i)_{\mathrm{dB}}-10\right|^2+\sum_{i=1}^{N}\left|S_{21}(f_i)_{\mathrm{dB}}\pm\delta\right|^2+\sum_{i=1}^{N}\left|\angle S_{21}(f_i)\pm 5\right|^2\right\}. \tag{7}$$

Since the frequency response over a wide bandwidth needs to be considered, and the number of circuit parameters exceeds the number of equations, the particle swarm optimization (PSO) method is utilized to obtain the optimized circuit parameters. Firstly, the center frequency f_0, transmission coefficient k, bandwidths and range of characteristic impedances are determined. Secondly, specific tolerances are assigned to the S-parameters according to the requirements, such as the amplitude imbalance δ of in-band transmission coefficient is less than 0.5 dB. The expression of the objective function O_b is shown in (7). The design objectives are as follows: the 3-dB passband bandwidth and the 10-dB impedance bandwidth for both the reference line and main line should exceed 70%, and the ±5° PD bandwidth should be greater than 40%. Figure 5 shows the optimization flowchart of PSO.

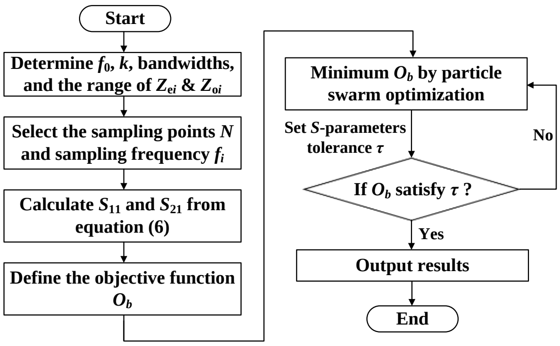

Fig. 5. The optimization flowchart of the PSO.

Taking a phase shift of $\Delta\Phi = 45°$ as an example, where θ_a is 22.5°, a corresponding set of circuit parameters can be obtained: $Z_{o1} = 25\ \Omega$, $Z_{o2} = 30\ \Omega$, $Z_{o3} = 30\ \Omega$, $\Delta Z_1 = 125\ \Omega$ ($\Delta Z_1 = Z_{e1} - Z_{o1} = Z_{e2} - Z_{o2} = Z_{e3} - Z_{o3}$), $Z_{o4} = 25\ \Omega$, $Z_{o5} = 30\ \Omega$, $Z_{o6} = 50\ \Omega$, $\Delta Z_2 = 160\ \Omega$ ($\Delta Z_2 = Z_{e4} - Z_{o4} = Z_{e5} - Z_{o5} = Z_{e6} - Z_{o6}$), $Z_a = 50\ \Omega$.

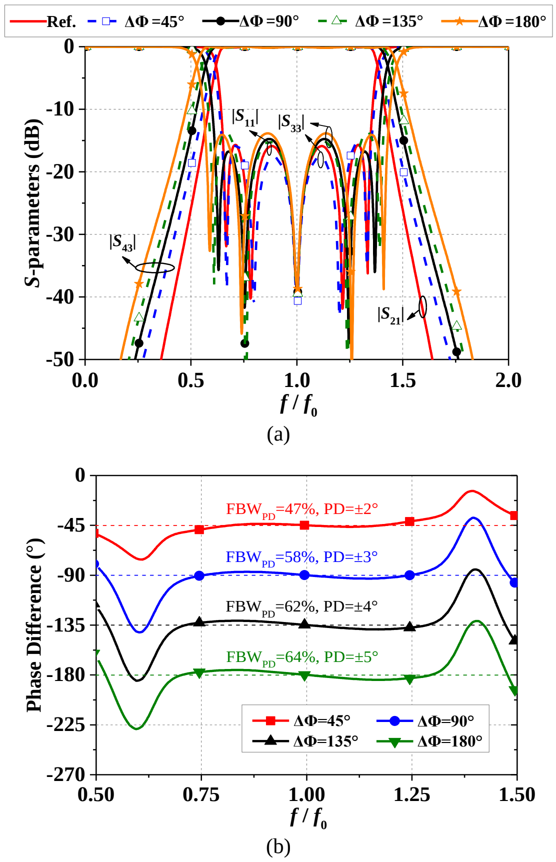

Fig. 6. Theory results of the proposed filtering D-PS. (a) S-parameters. (b) Phase difference.

To validate the phase shift range and filtering feature of the proposed multiway polyphase D-PS, Figure 6 displays the performances of the reference line and the main lines with different differential phase shifts. It can be observed that all D-PSs exhibit wide 3-dB passband bandwidth and wide 10-dB impedance bandwidth exceeding 70%, and the overlapped FBW of the filtering D-PS corresponding to PD values of −45°±2°, −90°±3°, −135°±4° and −180°±5° exceeds 45%.

Then, the circuit parameters of the reference line and main line that have significant impact on circuit performance are analyzed. For clarity, ΔZ_1 and ΔZ_2 are defined as the differences between the even- and odd-mode characteristic impedances of the asymmetrical TCL and CL in reference line, respectively. As exhibited in Fig. 7(a), both ΔZ_1 and Z_{o3} influence the impedance matching. As they increase, the 10-dB impedance bandwidth initially widens before decreases. In addition, Z_{o2} affects both reflection coefficient and transmission coefficient. As displayed in Fig. 7(b), the 10-dB impedance FBW improved from 14% to 71% when Z_{o2} increases from 10 Ω to 30 Ω, while decreases to 42% when Z_{o2} continues to increase to 40 Ω. As exhibited in Figs. 7(c) and 7(d), the parameters of CL have a more obvious impact on the overall performance. As ΔZ_2 or Z_{oc1} increases, both the 3-dB passband bandwidth and 10-dB impedance bandwidth first widen and then degrade. Moreover, the parameters affecting the PD bandwidth in main line are also investigated. As shown in Fig. 7(e), increasing either Z_{o6} or ΔZ_4 causes the slope of the PD to first flatten and then steepen, resulting the PD bandwidth that first widens and then narrows.

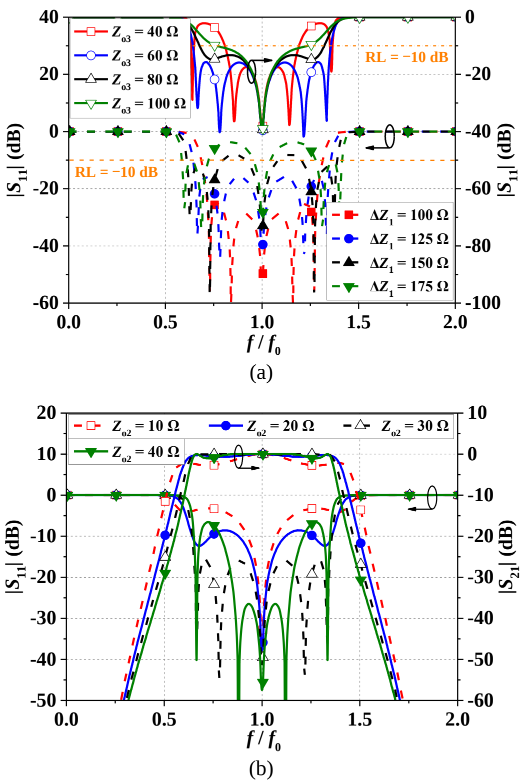

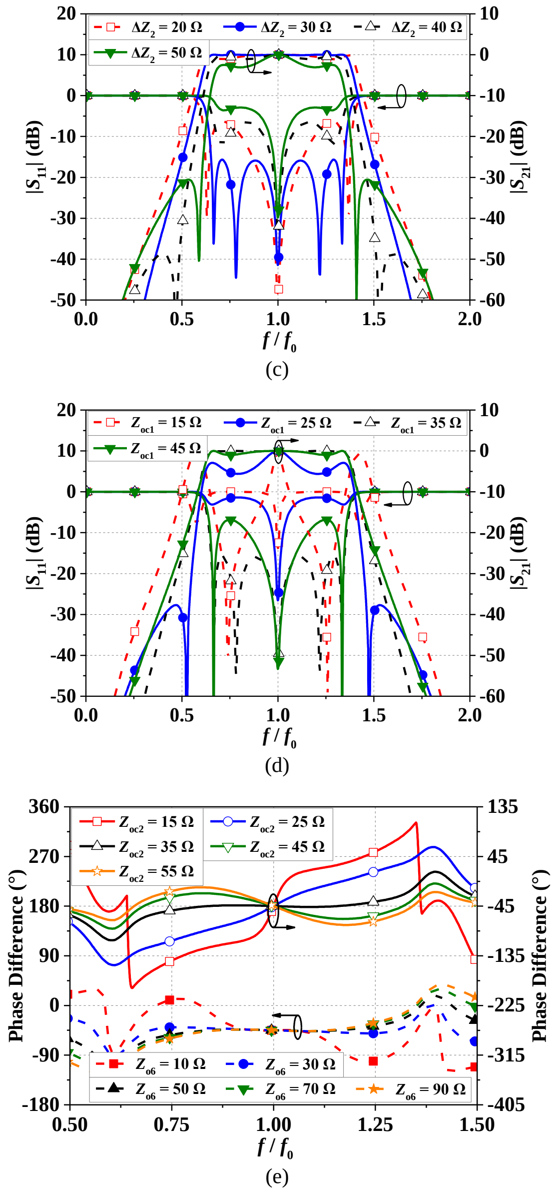

Fig. 7. Effects of (a) ΔZ_1 & Z_{o3}, (b) Z_{o2}, (c) ΔZ_2, (d) Z_{oc1}, (e) Z_{o6} & ΔZ_4 on the performance of the D-PS.

3. Implementation and Measurements

To validate the design, a 1×3 filtering BFN prototype operating at 2 GHz was manufactured on a Rogers 4350b substrate, which has ε_r of 3.48 and height of 1.524 mm. Next, the proposed BFN is modeled and optimized in Ansoft HFSS, and the overall simulated results can be obtained by combining the diode model in ADS. Figure 8 gives the layout with physical dimensions of the fabricated prototype, as well as photographs of it. The prototype occupies an area of 163 mm × 158 mm (1.1 λ_g × 1 λ_g). Detailed dimensions of the multiway polyphase filtering D-PSs are provided in Tab. 2. In the implementation, RF p-i-n diodes SMP1345-079LF are used as switches. It is noted that the section enclosed in purple dashed box corresponds to the additional multi-resonant absorption branch, which provides a reflectionless input signal for the subsequent stage of the filtering D-PS [19].

Subsequently, the fabricated prototype was measured using Agilent N5230A network analyzer, and measurements are plotted in Fig. 9. As shown in Fig. 9(a), when reference line, PS_1 and PS_4 are activated, the PDs of −30° and 150° can be realized by altering on/off states of the cascaded p-i-n diodes, denoted as state 1 and 2, respectively. These two states exhibit nearly identical reflection coefficients and transmission characteristics.

Reference Line	
Physical Dimensions	W_a = 0.1, W_b = 1.3, W_c = 0.1, W_d = 4.5, S_a = 0.1, S_b = 0.3, S_c = 1.8, L_a = 23, L_b = 22
Phase Shifter 1 ($\Delta\varphi_1$ = −30°)	
Physical Dimensions	W_a = 0.15, W_b = 1.35, W_c = 0.2, W_d = 4.7, W_e = 2.8, S_a = 0.1, S_b = 0.27, S_c = 1.6, L_a = 22.5, L_b = 20.8, L_c = 3.5
Phase Shifter 2 ($\Delta\varphi_2$ = −90°)	
Physical Dimensions	W_a = 0.15, W_b = 1.3, W_c = 0.4, W_d = 4.4 W_e = 3, S_a = 0.15, S_b = 0.17, S_c = 1.2, L_a = 22.5, L_b = 22, L_c = 11.4
Phase Shifter 3 ($\Delta\varphi_3$ = −120°)	
Physical Dimensions	W_a = 0.15, W_b = 1.35, W_c = 0.2, W_d = 4.7, W_e = 2.8, S_a = 0.1, S_b = 0.27, S_c = 1.6, L_a = 22.5, L_b = 20.8, L_c = 3.5
Phase Shifter 4 ($\Delta\varphi_4$ = −60°)	
Physical Dimensions	W_a = 0.15, W_b = 1.4, W_c = 0.2, W_d = 4.4, W_e = 2.8, S_a = 0.1, S_b = 0.2, S_c = 1.3, L_a = 22.5, L_b = 21, L_c = 7.4
Phase Shifter 5 ($\Delta\varphi_5$ = −180°)	
Physical Dimensions	W_a = 0.1, W_b = 1.3, W_c = 0.6, W_d = 4.3, W_e = 2.4, S_a = 0.3, S_b = 0.1, S_c = 2, L_a = 22.5, L_b = 21.3, L_c = 22.6

Tab. 2. Dimensions of the proposed multiway polyphase D-PSs (Unit: mm).

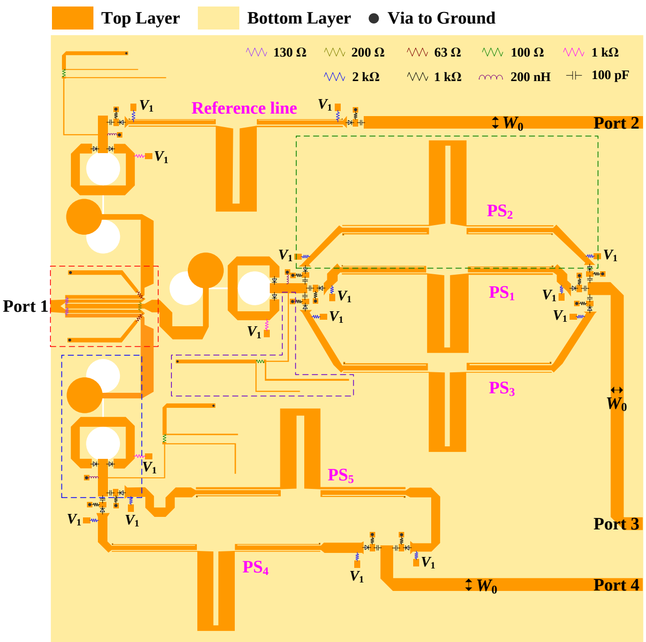

(a)

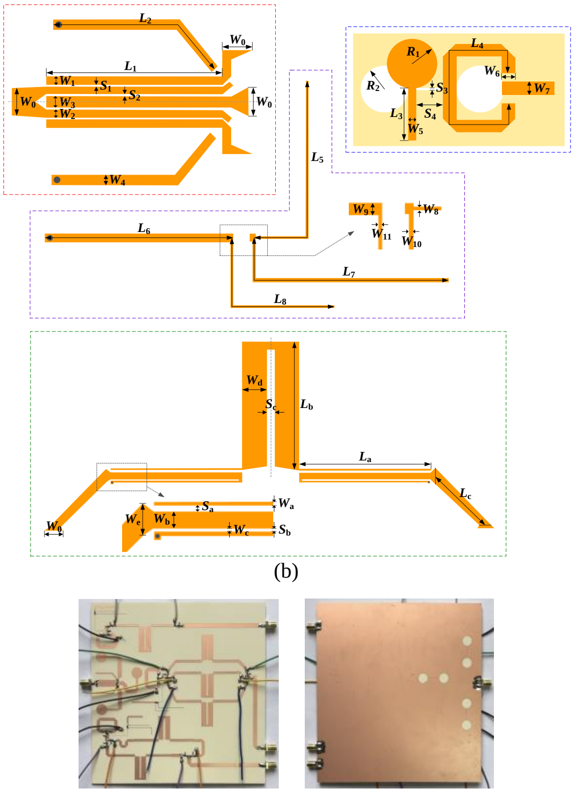

(b)

(c)

Fig. 8. Layout and photograph of the fabricated prototype. (a) Layout. (b) Partial enlarged view of the layout. (c) Top and bottom view of the fabricated prototype. (W_0 = 3.4 mm, W_1 = 1 mm, W_2 = 1 mm, W_3 = 1.2 mm, W_4 = 1 mm, W_5 = 1.6 mm, W_6 = 2.8 mm, W_7 = 3.2 mm, W_8 = 0.1 mm, W_9 = 1.4 mm, W_{10} = 0.3 mm, W_{11} = 0.2 mm, S_1 = 0.1 mm, S_2 = 0.2 mm, S_3 = 0.1 mm, S_4 = 6.5 mm, L_1 = 20 mm, L_2 = 22 mm, L_3 = 10 mm, L_4 = 47.6 mm, L_5 = 24 mm, L_6 = 21.5 mm, L_7 = 28 mm, L_8 = 20 mm, R_1 = 4.8 mm, R_2 = 4.5 mm).

Similarly, the combinations of reference line with PS_2 and PS_5, and the reference line with PS_3 and PS_4, generate output PDs of −90° and 90°, −120° and 60°, respectively, referred to as states 3-6. As displayed in Figs. 9(b) and 9(c), the measured reflection coefficients are below −10 dB across the entire band, and the 3-dB passband bandwidth ranges can cover 1.24 GHz to 2.66 GHz. Furthermore, as displayed in Figs. 9(d) and 9(e), the measured ±7° PD bandwidth exceeds 40%, covering the frequency range of 1.6 GHz ~ 2.4 GHz.

Table 3 presents the comparisons between the proposed and state-of-the-art BFNs. Firstly, the proposed BFN achieves wideband filtering response with input reflectionless feature, while others show none of the two feature or only filtering performance. In addition of this, the proposed BFN exhibits lower PD error, flatter amplitude imbalance, and more compact size when compared with the PD reconfigurable BFNs in [12], [13], and [14]. Moreover, it exhibits the widest 3-dB passband bandwidth and can provide more beams than the filtering BFNs in [15] and [17]. In this section, the parameters that have major influences on the FPD are analyzed for better illustration.

Ref.	Network Type	Num. of Phase State	PD error (°)	IL (dB)	Filtering Function	Reflectionless	FBW (%)		RC	Num. of Layers	Size ($\lambda_g \times \lambda_g$)
							$\|S_{11}\| < -10$ dB	3-dB passband			
[12]	4×4	8	±10	2.2±1.8	No	No	20	/	/	1	2.8 × 1.4
[13]	4×4	12	±12	1.8±1.7	No	No	33.3	/	/	1	1.6 × 1.3
[14]	3×3	6	±8.5	1.4±0.9	No	No	19	/	/	1	2.4 × 1.1
[15]	4×4	4	±10	0.7±0.7	Yes	No	9.6	7.5	1.8*	3	1.4 × 0.7*
[17]	3×3	3	±5	1.4±1	Yes	No	51.4	70.3	1.26	1	0.5 × 0.5
This Work	**1×3**	**6**	**±7**	**2.3±0.5**	**Yes**	**Yes**	**All band**	**71**	**1.35**	**1**	**1.1 × 1**

PD: Phase difference; IL: Insertion loss (the losses introduced by switches are included); FBW: Fractional Bandwidth; RC: Rectangle Coefficient = $|BW_{20dB}/BW_{3dB}|$; *: Estimated value.

Tab. 3. Comparisons between the proposed and other reported state-of-the-art BFNs.

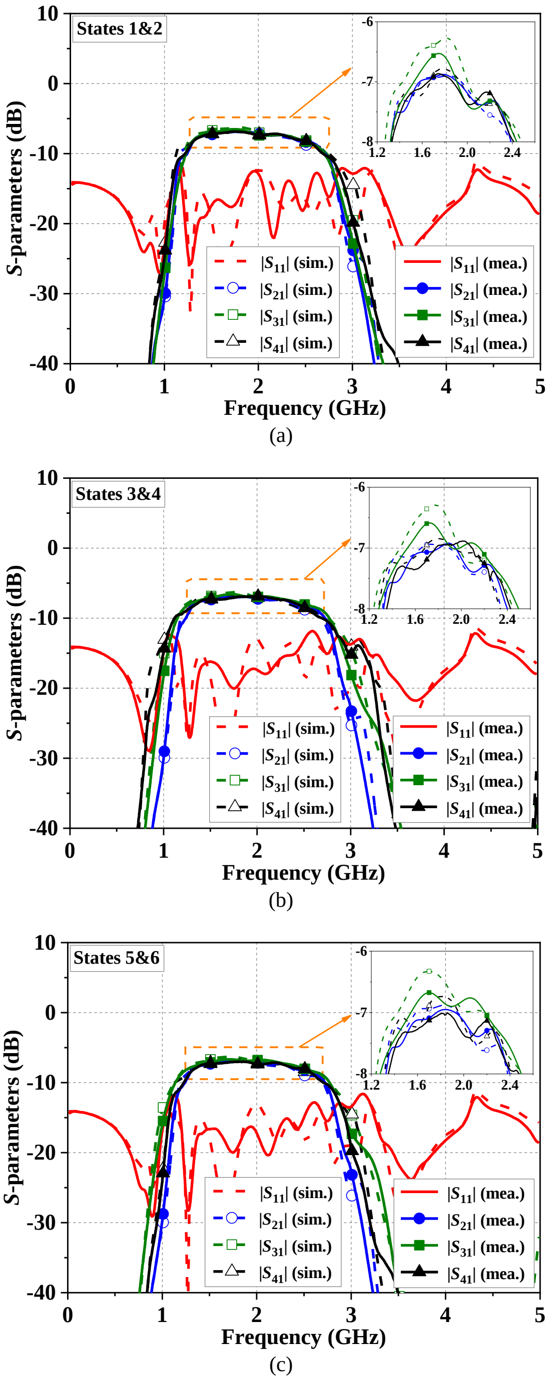

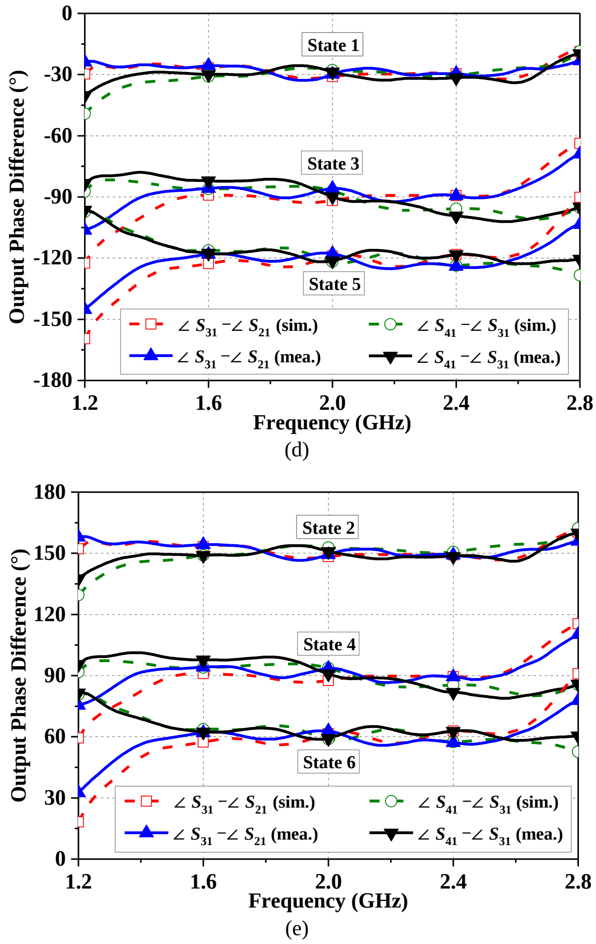

Fig. 9. Simulated and measured results of the fabricated 1×3 BFN. (a–c) *S*-parameters on states 1&2, 3&4, and 5&6. (d–e) Phase differences between output ports on states 1&3&5, and 2&4&6.

4. Conclusions

A wideband 1×3 filtering BFN with extended phase reconfigurability and input-reflectionless feature is proposed and experimentally validated. Six distinct output PDs are realized using only three groups of D-PSs in a network comprising a three-way reflectionless power divider, switched 0°/180° PSs, and multiway polyphase D-

PSs, providing wideband filtering, high selectivity, and input-reflectionless performances. The prototype achieves a 3-dB passband over 70%, $|S_{11}|$ below –10 dB, and a ±7° PD error bandwidth of 40%. The proposed BFN is an effective solution for multi-beam antenna systems that require wideband operation, multiple beam directions, and high-performance filtering in a compact and flexible configuration.

Acknowledgments

This work was supported in part by the National Natural Science Foundation of China under Grant 52471371, in part by the China Scholarship Council under Grant 202406570025, in part by the Young Elite Scientists Sponsorship Program by CAST under Grant 2022QNRC001 and in part by the Fundamental Research Funds for the Central Universities under Grant 3132026230. (Corresponding author: Hongmei Liu.)

References

[1] TRZEBIATOWSKI, K., KALISTA, W., RZYMOWSKI, M., et al. Multibeam antenna for Ka-band CubeSat connectivity using 3-D printed lens and antenna array. *IEEE Antennas and Wireless Propagation Letters*, 2022, vol. 21, no. 11, p. 2244–2248. DOI: 10.1109/LAWP.2022.3189073

[2] ZHANG, Y. J., HAN, Z. X., TANG, S. W., et al. A highly pattern-reconfigurable planar antenna with 360° single- and multi-beam steering. *IEEE Transactions on Antennas and Propagation*, 2022, vol. 70, no. 8, p. 6490–6504. DOI: 10.1109/TAP.2022.3161514

[3] GUO, C. A., GUO, Y. J. A general approach for synthesizing multibeam antenna arrays employing generalized joined coupler matrix. *IEEE Transactions on Antennas and Propagation*, 2022, vol. 70, no. 9, p. 7556–7564. DOI: 10.1109/TAP.2022.3153037

[4] DENG, J. Y., ZHANG, Y., LIN, W. Compact multibeam antenna array facilitated by miniaturized slow wave substrate integrated waveguide Butler matrix. *IEEE Transactions on Antennas and Propagation*, 2024, vol. 72, no. 12, p. 9564–9569. DOI: 10.1109/TAP.2024.3463203

[5] DUTTA, R. K., JAISWAL, R. K., SIAKIA, M., et al. A two-stage beamforming antenna using Butler matrix and reconfigurable frequency delective surface for wide angle beam tilting. *IEEE Antennas and Wireless Propagation Letters*, 2023, vol. 22, no. 10, p. 2342–2346. DOI: 10.1109/LAWP.2023.3286819

[6] YANG, Y., XU, B. W., CHAN, W. S., et al. Reconfigurable single/dual-beam steering based on compact 3×3 Nolen matrix with equal/unequal power division and phase difference. *IEEE Antennas and Wireless Propagation Letters*, 2024, vol. 23, no. 11, p. 3724–3728. DOI: 10.1109/LAWP.2024.3427341

[7] XU, Y., ZHU, H., GUO, Y. J. Compact wideband 3×3 Nolen matrix with couplers integrated with phase shifters. *IEEE Microwave and Wireless Technology Letters*, 2024, vol. 34, no. 2, p. 159–162. DOI: 10.1109/LMWT.2023.3341791

[8] WANG, X. Z., CHEN, F. C., CHU Q. X. A compact broadband 4×4 Butler matrix with 360° continuous progressive phase shift. *IEEE Transactions on Microwave Theory and Techniques*, 2023, vol. 71, no. 9, p. 3906–3914. DOI: 10.1109/TMTT.2023.3249352

[9] CHU, H. N., HOANG, T. H., JI, K. J., et al. A phase distribution network using 2×4 Butler matrix for linear/planar beam-scanning arrays. *IEEE Access*, 2021, vol. 9, p. 133438–133448. DOI: 10.1109/ACCESS.2021.3115880

[10] YU, D., LIU, H. M., LI, S., et al. Control-relaxed wideband 2×4 Nolen matrix with 360° continuously tuned differential phase. *IEEE Transactions on Circuits and Systems II: Express Briefs*, 2024, vol. 71, no. 4, p. 1979–1983. DOI: 10.1109/TCSII.2023.3334248

[11] REN, H., LI, P. Z., GU, Y. X., et al. Phase shifter-relaxed and control-relaxed continuous steering multiple beamforming 4×4 Butler matrix phased array. *IEEE Transitions on Circuits and Systems I: Regular Papers*, 2020, vol. 67, no. 12, p. 5031–5039. DOI: 10.1109/TCSI.2020.3009215

[12] TAJIK, A., ALAVIJEH, A. S., FAKHARZADEH, M. Asymmetrical 4×4 Butler matrix and its application for single layer 8×8 Butler matrix. *IEEE Transactions on Antennas and Propagation*, 2019, vol. 67, no. 8, p. 5372–5379. DOI: 10.1109/TAP.2019.2916695

[13] DING, K. J., KISHK, A. A. Extension of Butler matrix number of beams based on reconfigurable couplers. *IEEE Transactions on Antennas and Propagation*, 2019, vol. 67, no. 6, p. 3789–3796. DOI: 10.1109/TAP.2019.2902668

[14] LIU, H. W., GU, X. Y., TIAN, H. L. Design of extended Nolen matrix with enhanced beam controllability and widened spatial coverage. *IEEE Transactions on Circuits and Systems II: Express Briefs*, 2024, vol. 71, no. 7, p. 3273–3277. DOI: 10.1109/TCSII.2024.3362148

[15] SHAO, Q., CHEN, F. C., WANG, Y., et al. Design of 4×4 and 8×8 filtering Butler matrices utilizing combined 90° and 180° couplers. *IEEE Transactions on Microwave Theory and Techniques,* 2021, vol. 69, no. 8, p. 3842–3852. DOI: 10.1109/TMTT.2021.3085879

[16] SHAO, Q., CHEN, F. C., WANG, Y., et al. Design of modified 4×6 filtering Butler matrix based on all-resonator structures. *IEEE Transactions on Microwave Theory and Techniques*, 2019, vol. 67, no. 9, p. 3617–3627. DOI: 10.1109/TMTT.2019.2925113

[17] ZHANG, Y., LIU, H. M., LI, S., et al. Design of highly integrated wideband 3×3 Nolen matrix using arbitrary-phase-difference filtering couplers and phase compensation networks. *International Journal of Microwave and Wireless Technologies*, 2025, vol. 17, no. 6, p. 1041–1051. DOI: 10.1017/S1759078725102407

[18] ZHANG, Y., LIU, H. M., CHEN, S. Y., et al. All-port-reflectionless wideband filtering power divider using five-line coupled structure. *IEEE Microwave and Wireless Technology Letters,* 2025, vol. 35, no. 1, p. 31–34. DOI: 10.1109/LMWT.2024.3471828

[19] ZHANG, S. R., LIU, H. M., WANG, Z. B., et al. Design of wideband quasi-reflectionless filter with high selectivity and flat passband. *IEEE Transactions on Circuits and Systems II: Express Briefs*, 2023, vol. 70, no. 11, p. 4038–4042. DOI: 10.1109/TCSII.2023.3284420

[20] ZHU, H., CHENG, Z. Q., GUO, Y. J. Design of wideband in-phase and out-of-phase power dividers using microstrip-to-slotline transitions and slotline resonators. *IEEE Transactions on Microwave Theory and Techniques*, 2019, vol. 67, no. 4, p. 1412 to 1424. DOI: 10.1109/TMTT.2019.2897928

[21] BIALKOWSKI, M., ABBOSH, A. M. Design of a compact UWB out-of-phase power divider. *IEEE Microwave and Wireless Components Letters*, 2007, vol. 17, no. 4, p. 289–291. DOI: 10.1109/LMWC.2007.892979

[22] POZAR, D. M. *Microwave Engineering.* 3rd ed. New York (NY, USA): Wiley, 2005. ISBN: 978-0471448785

About the Authors ...

Yan ZHANG was born in Shanxi, China. She received the B.S. degree in Communication Engineering from Dalian Jiaotong University (DJTU), China, in 2018, and the Master degree in Electronic and Communication Engineering from Dalian Maritime University (DMU), China, in 2021. She is currently pursuing the Ph.D. degree at DMU. Her research interests include function fusion microwave circuits and beamforming networks.

Hongmei LIU (Member, IEEE, corresponding author) received the Ph.D. degree in Information and Communication Engineering from Dalian Maritime University (DMU), China, in 2016. She is currently a Full Professor with the School of Information Science and Technology, DMU. Her current research interests include CP antennas, multi-function microwave circuits, reconfigurable RF components, and multi-beam antennas. She has authored or co-authored over 90 papers in journals and conferences. She is currently serving as a Technical Reviewer for the IEEE Transactions on Microwave Theory and Techniques, IEEE Transactions on Circuits and Systems, IEEE Transactions on Industrial Electronics, IEEE Microwave and Wireless Components Letters, IET Microwaves, Antennas & Propagation, International Journal of RF and Microwave Computer-Aided Engineering, and AEU-International Journal of Electronics and Communications. She was a recipient of the Best Doctor's Dissertation Award of Liaoning Province in 2017.

Yao MENG was born in Dalian, China. She received the B.S. degree in Electronic and Information Engineering from University of Science and Technology Liaoning (USTL), China, in 2024. She is currently pursuing the Master's degree at Dalian Maritime University (DMU). Her current research interests include beamforming network and patch antennas.

Zhongbao WANG (Member, IEEE) received the Ph.D. degree in Communication and Information Systems from DMU, China, in 2012. He is currently a Full Professor with the School of Information Science and Technology, DMU. From 2014 to 2018, he was a Postdoctoral Fellow with Beijing University of Posts and Telecommunications, China. From 2019 to 2020, he was a Visiting Scholar with National University of Singapore, Singapore. He has authored more than 90 journal papers. He is currently serving as a Technical Reviewer for the IEEE Transactions on Circuits and Systems, MTT, MWTL, Radioengineering, and so on. His current research interests include balanced RF components and CP antennas.